Hindawi
Advances in Materials Science and Engineering
Volume 2018, Article ID 9691856, 8 pages
https://doi.org/10.1155/2018/9691856

Research Article

$(Co,Mn)_3O_4$ Spinel Coating for Protecting Metallic Interconnects Thermally Converted from an Electro-Codeposited Co-Mn_3O_4 Composite Coating

Yelong Li,[1] Jianli Song,[2] Jiahong Zhu,[3] Yongtang Li,[1] and Wen Yang[1]

[1]*School of Materials Science and Engineering, Taiyuan University of Science and Technology, Taiyuan 030024, China*
[2]*School of Instrument Science and Opto Electronics Engineering, Beijing Information Science and Technology University, Beijing 100192, China*
[3]*Department of Mechanical Engineering, Tennessee Technological University, Cookeville, TN, USA*

Correspondence should be addressed to Jianli Song; songjianli@bistu.edu.cn

Received 7 May 2018; Revised 2 July 2018; Accepted 19 July 2018; Published 14 August 2018

Academic Editor: Simo-Pekka Hannula

Electro-codeposition was used to prepare the Co and Co-Mn_3O_4 precursor coatings on ferritic stainless steel E-brite. Plated samples were exposed at 800°C in air for different durations (i.e., 10 min and 4 h) for thermal conversion of the deposited layer to a spinel coating. The converted layer was characterized with scanning electron microscopy/energy-dispersive spectroscopy (SEM/EDS) and X-ray diffraction (XRD). The results showed that after 10 min heat treatment, the plated Co layer was not fully oxidized and converted into a double-layer microstructure with an inner CoO layer and outer Co_3O_4 layer, while for the Co-Mn_3O_4 layer, the Mn_3O_4 particles were not completely dissolved into the oxide layer. After 4 h of exposure, the surface layer was fully converted into the Co_3O_4 or $(Co,Mn)_3O_4$ spinel coating. Though the Mn content in $(Co,Mn)_3O_4$ was relatively low, the Mn-doped spinel coating was advantageous over the pure cobalt spinel coating, as the thermally grown Cr_2O_3 scale at the coating/substrate interface was more compact and protective. Co diffusion from the deposited layer into the alloy substrate was observed for both coatings.

1. Introduction

The ferritic stainless steel (FSS) with the $(Co,Mn)_3O_4$ spinel coating is considered as one of the best material systems for intermediate-temperature solid oxide fuel cell (SOFC) interconnects [1–3]. Compared with the ceramic interconnects, the FSS has the advantage of low cost, excellent electrical conductivity, and thermal expansion which can meet the physical performance requirement of the fuel cell [4–6]. The $(Co,Mn)_3O_4$ spinel coating can effectively block the outward migration of volatile Cr from the substrate which will result in the Cr poisoning of the SOFC cathode [7–9]. One of the most promising methods for synthesis of the $(Co,Mn)_3O_4$ spinel coating is deposition of a Co-Mn precursor layer on the surface of the substrate, which is then thermally converted into a spinel phase by heat treatment in air. In recent years, several routes for preparation of the Co-Mn precursor layer were explored, including screen printing [10], physical vapor depositions (PVD) such as sputtering [11], sol-gel spray painting [12], and electroplating of the Co-Mn alloy layer [13, 14]. Screen printing and sputtering are both line-of-sight processes not suitable for coating complex-shaped interconnects. The layer prepared by spray painting needs a high sintering temperature to achieve a proper coating density [12], and the high temperature could negatively affect the microstructure and performance of the interconnects. In general, electroplating is one of the most effective and promising methods, offering advantages such as low manufacturing cost, decent coating quality, and ready adaptation to corrugated shape of the interconnects. However, there are still some technical problems to be solved, including the appearance of $Mn(OH)_2$ in the

electroplating process as well as a significant deposition standard potential difference between Co and Mn [$E^o(Mn^{2+}/Mn) = 1.18$ V, $E^o(Co^{2+}/Co) = 0.28$ V]. Therefore, electrolytic codeposition (also called electro-codeposition) is considered to be a better approach to solve these problems. In this method, the desired particles are dispersed in the electrolyte and are incorporated into the growing metal layer during electroplating, thus forming the metal matrix composite coatings. In the subsequent heat treatment (also called thermal conversion) step, a single-phase oxide coating can be obtained due to the interaction and reaction among the particles, metal matrix, and oxygen in air. Apelt et al. [15] synthesized composite coatings consisting of the Co matrix and Mn_3O_4 particles and optimized the process parameters. However, thermal conversion of the composite layer into a spinel coating has rarely been studied and reported yet.

In this work, the Mn_3O_4 particles were dispersed in a Co-plating solution and embedded in the Co coating during the plating process. The Co-Mn_3O_4 composite coating was then transformed into $(Co,Mn)_3O_4$ spinel coating by thermal conversion. The surface and cross-sectional features of the coatings before and after the thermal conversion were observed and characterized, and a pure Co coating was included in the evaluation for comparison.

2. Experiment

In this research, the ferritic stainless steel E-brite (Allegheny Ludlum) was chosen as the alloy substrate, and the composition is listed in Table 1.

E-brite coupons measuring approximately 20 mm × 15 mm were cut from a 1.65 mm thick sheet metal using a shearing machine. A hole of 1.5 mm in diameter was then drilled for hanging the coupon in the heat-treating furnace. The coupons were mechanically polished with various grades of silicon carbide papers up to 600 grit, followed by ultrasonic cleaning in water and acetone.

In order to remove the native oxide layer on the surface of the coupons and increase the surface roughness and promote the adhesion of the electrodeposited layer, anode activation and strike plating were conducted prior to electroplating [13]. The device for anode activation was the same as electroplating, using pure Co plate as the cathode and the coupon as anode. The solution composition and time for anode activation, pure cobalt plating, and Mn_3O_4-Co electrolytic codeposition are shown in Table 2. The particle size of Mn_3O_4 (US Research Nanomaterials, Inc) used in the experiment was about 2.5 μm. All experiments were carried out with 300 ml electrolyte prepared with deionized water, and the applied current density was 20 mA/cm^2. All processes were conducted at room temperature with continuous stirring to ensure that all ingredients (including the Mn_3O_4 particles) were homogeneously distributed in the solution.

To study the progression of the thermal conversion, the coated coupons were heated in a box furnace to 800°C in stagnant air at a heating rate of 1°C/min and held at 800°C for either 10 min or 4 h, and then the furnace was cooled to room temperature. For cross-sectional observation, the coated and converted coupons were electroplated with a layer of copper for enhanced edge retention. After mounting in an acrylic-based resin, the coupons were grinded and polished for the cross-sectional analysis.

Surface and cross-sectional features were observed with scanning electron microscopy (SEM, from JOEL) equipped with an Oxford INCA unit for energy dispersive spectroscopy (EDS). The phases in the thermally converted coatings were determined using X-ray diffraction (XRD, PANalytical X'pert) with a Cu target. Measurements were taken in a 2θ range of 20°–80° with a step size of 0.05° and a step time of 0.3 s.

3. Results and Discussion

3.1. Examination of the As-Deposited Coatings. The surface features of both pure Co coating and Co-Mn_3O_4 composite coating are shown in Figure 1.

After 10 min plating, E-brite was completely covered with cobalt. As shown in Figure 1(a), the grains of Co were slender spindle shaped of approximately 2~3 μm long and with a random direction. The Co-Mn_3O_4 composite coating is similar to pure Co but contains a number of Mn_3O_4 particles with an irregular shape (Figure 1(b)). The cross section of the Co-Mn_3O_4 composite coating is presented in Figure 2. The middle layer is the composite coating with a thickness of about 8 μm. The dark Mn_3O_4 particles were distributed reasonably and uniformly in the coating, and there was no obvious particle agglomeration. And the coating was well adherent to the substrate.

3.2. Surface Morphology of the Converted Coatings. Figure 3 shows the surface images of the cobalt layer after thermal conversion for different times. When the sample was just held for 10 min at 800°C, the oxidized cobalt grains changed into the cobble shape which was completely different from that of the as-deposited layer. After thermal exposure at 800°C in air for 4 h, the grains of the oxidized cobalt grew to nearly 1 μm much larger than that exposed for 10 min. There was no visible porosity, cracks, or other defects on the appearance surface of converted pure Co plating.

The surface features of the converted Co-Mn_3O_4 composite coating are shown in Figure 4. The overall surface was not as flat as the oxidized cobalt layer because of the implanted Mn_3O_4 particles. The morphology of the oxide converted from cobalt in the composite was similar to that in the pure cobalt layer. With the addition of the Mn_3O_4 particles, the thermal conversion of coatings was more complex, which is impacted by the interactions between Mn-containing oxide particles, Co, and the oxygen from the conversion environment. After 10 minutes of oxidation, the $(Co,Mn)_3O_4$ spinel could be formed near the matrix-particle interface. However, due to the short exposure time, the Mn_3O_4 particles did not completely incorporate into the surrounding coating. The light parts in Figures 4(a) and 4(b) are the incompletely converted Mn_3O_4 particles not embedded completely inside the original cobalt layer. In the high-magnification image shown in Figure 4(b), the crystalline facets associated with a Mn_3O_4 particle were visible clearly.

Table 1: Chemical composition (wt.%) of the E-brite substrate alloy.

Fe	Cr	Mn	C	P	S	Ni	Al	Mo	Cu	Cb	N	Si
Balance	26.05	0.06	0.002	0.013	0.013	0.12	0.002	1.01	0.01	0.12	0.011	0.13

Table 2: Solution composition and time for anodic activation, pure cobalt plating, and Mn_3O_4-Co electrolytic codeposition.

	Anodic activation/strike plating	Co plating	Mn_3O_4-Co plating
$CoCl_2{\cdot}6H_2O$	100 g/l	50 g/l	50 g/l
$CoSO_4{\cdot}7\ H_2O$	—	300 g/l	300 g/l
H_3BO_3	—	30 g/l	30 g/l
SDS	—	0.03 g/l	0.03 g/l
Mn_3O_4	—	—	120 g/l
HCl	85 ml/l	—	—
Time	2 min/6 min	10 min	10 min

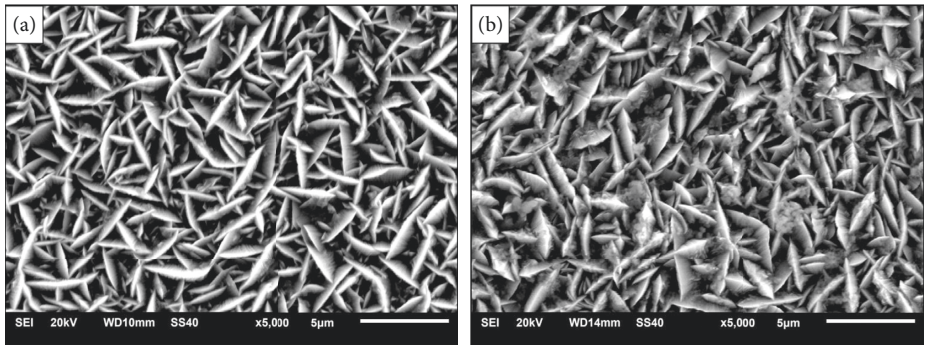

Figure 1: Surface morphology of the as-deposited coatings: (a) pure Co coating and (b) Co-Mn_3O_4 coating.

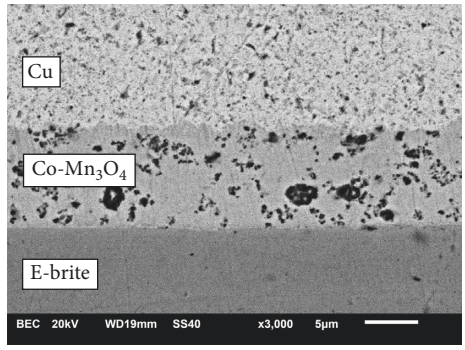

Figure 2: Cross-sectional morphology of the as-deposited Co-Mn_3O_4 composite coating by electro-codeposition.

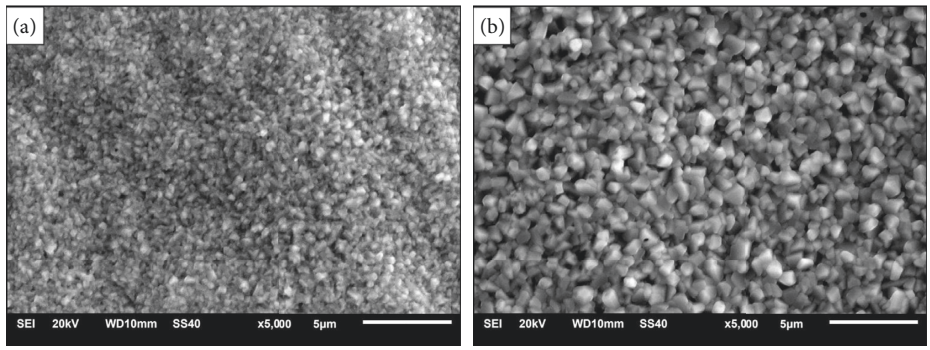

Figure 3: Surface morphology of the pure Co layer after oxidation for different times: (a) 10 min and (b) 4 h.

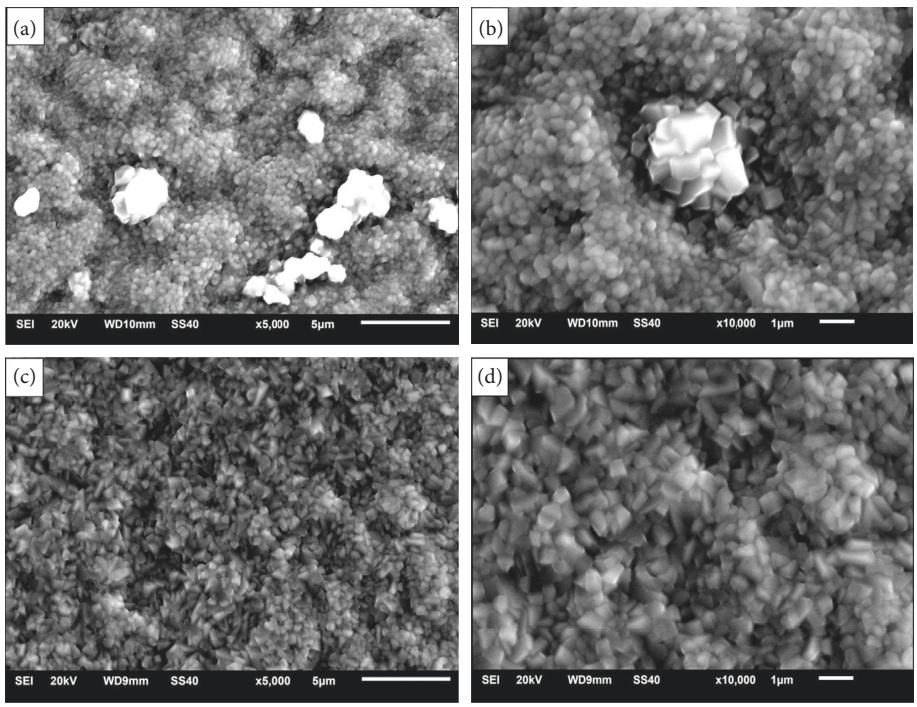

FIGURE 4: Surface morphology of Co-Mn_3O_4 composite coating after oxidization for different times: (a) 10 min, low magnification; (b) 10 min, high magnification; (c) 4 h, low magnification; (d) 4 h, high magnification.

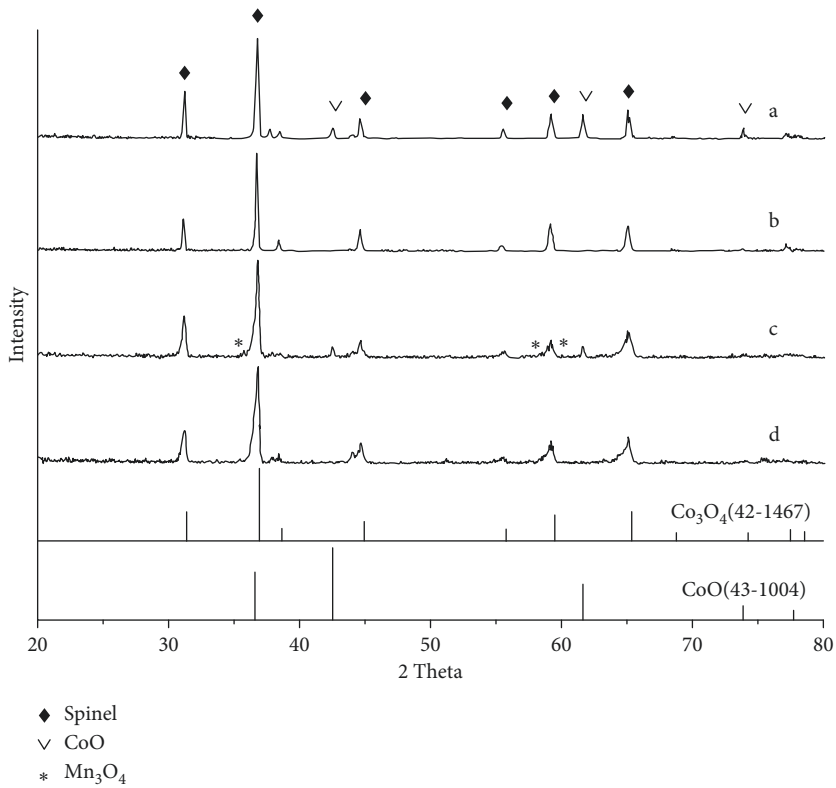

FIGURE 5: XRD patterns of the coatings after conversion for different times: (a) the Co coating for 10 min; (b) the Co coating for 4 h; (c) the Co-Mn_3O_4 coating for 10 min; and (d) the Co-Mn_3O_4 coating for 4 h. Cross-sectional examination of the converted coatings.

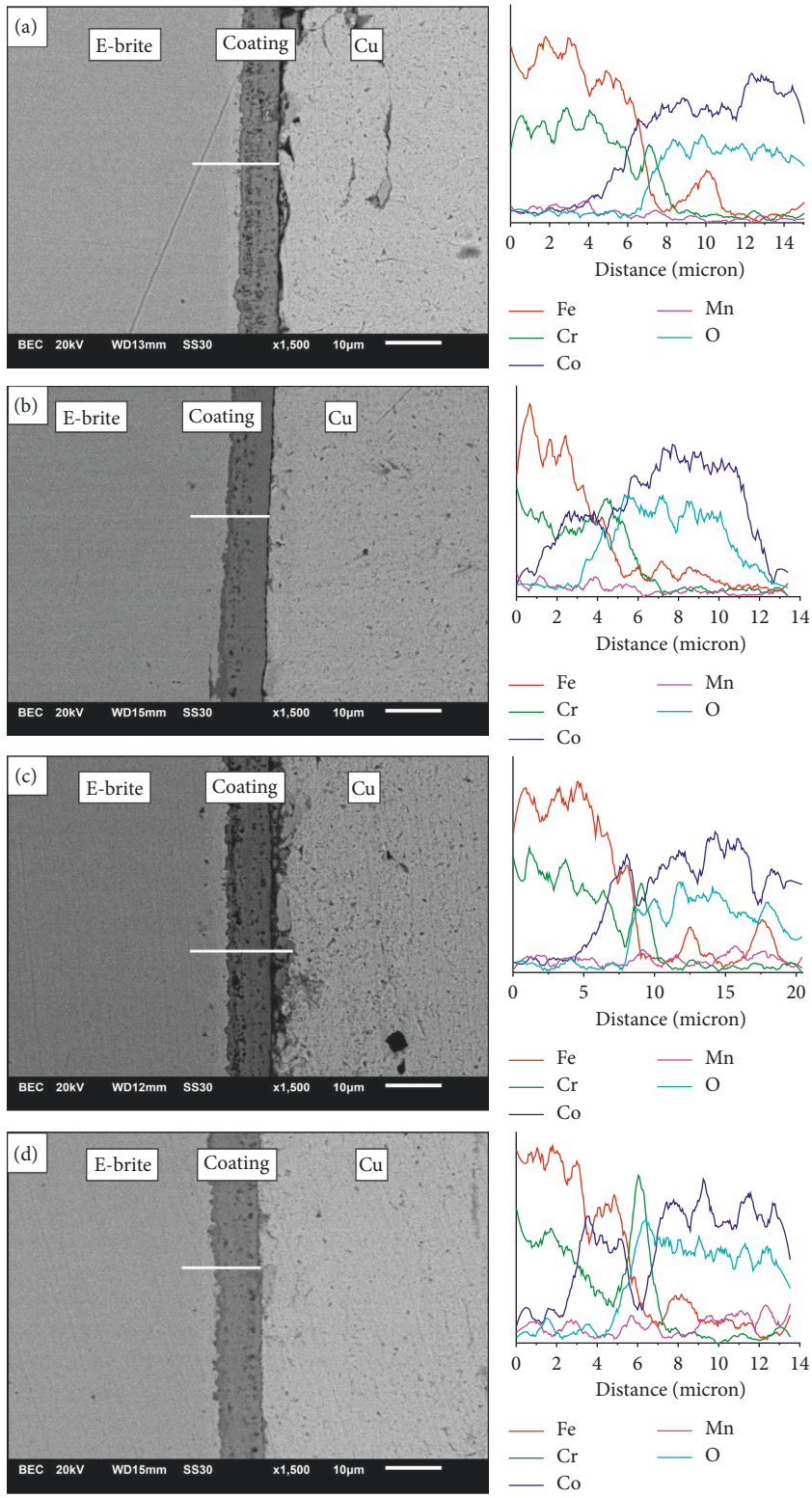

FIGURE 6: Cross-sectional morphology and EDS linear scan of the plated substrates after thermal conversion for different times: (a) the Co coating for 10 min; (b) the Co coating for 4 h; (c) the Co-Mn_3O_4 coating for 10 min; and (d) the Co-Mn_3O_4 coating for 4 h.

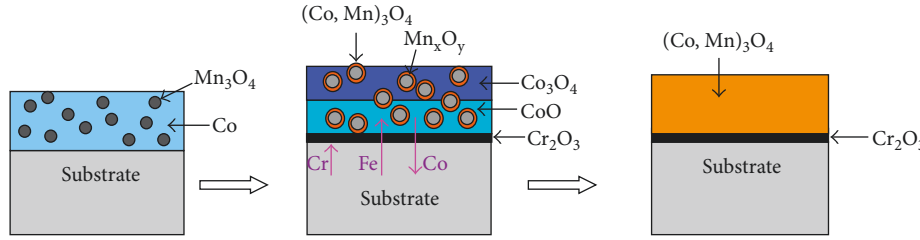

Figure 7: Sketches illustrating the process of thermal conversion of the Co-Mn_3O_4 composite coating to the $(Co,Mn)_3O_4$ spinel coating.

For the composite coating exposed for 4 h, there was no visible Mn_3O_4 particle on the surface. Apparently, the Mn_3O_4 particles had reacted completely with the cobalt oxide to form the Mn-containing spinel layer.

3.3. Phase Structures in the Converted Coatings. Figure 5 shows the XRD patterns of the coatings after thermal conversion at 800°C for different times. After conversion for 10 min, both Co_3O_4 and CoO peaks can be observed for the pure cobalt coating (Figure 5(a)). As such a double-layer microstructure with a surface Co_3O_4 layer and an inner CoO layer in contact with the Co substrate has been widely reported for pure cobalt samples oxidized at a temperature below 900°C [16, 17]. The growth of the two oxide layers is controlled by the diffusion of Co and oxygen ions through the generated oxide scale. Both Co_3O_4 and CoO have a cubic structure. The whole Co_3O_4 has a spinel structure with the space group of *Fd3m(227)*, and CoO has a rock salt structure with the space group of *Fm3m(225)*. After 4 h conversion, the diffraction peaks only existed in the Co_3O_4 pattern, as shown in Figure 5(b), indicating that the surface layer was completely oxidized to the stable spinel structure.

For the Co-Mn_3O_4 coating, after conversion for 10 min, the peaks from Co_3O_4, CoO, and Mn_3O_4 can be detected (Figure 5(c)). Similar to the Co layer, the short-term conversion led to the formation of the double-layered Co_3O_4/CoO microstructure. However, Mn_3O_4 peaks were also observed, due to the presence of the Mn oxide particles in the coating, which was coinciding with the results shown in Figures 4(a) and 4(b). It should be noted that the peaks of Mn_3O_4 particles were pretty weak, as a result of the relatively low particle incorporation in the plated layer. It has initially transformed to Mn_2O_3 and interacted/reacted with Co_3O_4 to form the $(Co,Mn)_3O_4$ spinel at this temperature. After conversion for 4 h of the Co-Mn_3O_4 coating, only a spinel phase was present in the surface coating (Figure 5(d)); during this period, the reaction and formation of the $(Co,Mn)_3O_4$ spinel is completed. The XRD lines of the converted Co-Mn_3O_4 composite coating is little different from those of the converted cobalt coating, as all of the peaks were more broadened. This is due to the nonuniform incorporation of Mn into Co_3O_4, forming the $(Co,Mn)_3O_4$ spinel with slightly varied compositions.

Figure 6 shows the cross-sectional morphologies and EDS line scans of the plated substrates after conversion. The thickness of the converted coatings was slightly larger than that of the as-deposited layer, and this is associated with an increased molar volume of the product. Based on the results of EDS line scans, after 10 min at 800°C, Cr had already diffused outward from the FSS substrate to the surface to form an oxide layer at the interface between the substrate and coating in all samples. This oxide layer contained not only Cr and O, but also Co, as well as some Fe in the Co-plated samples, likely due to the extremely thin nature of the formed Cr_2O_3 scale. With the extended conversion time, more Cr was detected in the scale, but the thickness of the scale maintained 2-3 μm in all samples after 4 h conversion. The inner layer of the coating indirectly in contact with the substrate in the composite coating samples was mainly composed of manganese-chromium spinel, while in the pure Co-plated samples, there was still a significant amount of Fe in the scale. The Cr content was very low near the surface of each spinel layer, implying that the converted layers, regardless of whether Mn is contained, during this period of oxidation, had the capability of blocking the evaporation of Cr from the FSS substrate. It was obvious that the Cr_2O_3 scale in the $(Co,Mn)_3O_4$ spinel coating was more compact and contained less Fe than that in the Co_3O_4 coating. The compact oxide layer can prevent further oxidation, and it is of great significance for the long-term performance stability of SOFC running at elevated temperatures.

Similar to Cr, some Fe also diffused outward from the substrate to the coating. According to the EDS results, the diffusion distance of Fe was further than that of Cr at the same time, implying that the diffusivity of Fe is greater than that of Cr, which agrees with the data in the literature [18]. With the extended conversion time, Fe was more uniformly dispersed in the coating. It appears that the converted composite coating contained more Fe than the converted Co coating.

From Figure 6, the inward diffusion of Co from the coating to the substrate was also observed for both the Co and Co-Mn_3O_4 coatings after the conversion treatment. The interdiffusion between the coating and the substrate led to the formation of Kirkendall voids in the coating. Since these voids/porosities are relatively small and not interconnected, their potential impact on the performance of the plated metallic interconnect is expected to be minimal. On the contrary, the Co incorporation in the FSS matrix near the substrate/coating interface will lead to the transformation of the body-centered cubic (BCC) structure into the face-centered cubic (FCC) structure in this region. The FCC structure has a much higher coefficient of thermal expansion (CTE) than that of the BCC structure as well as those of the adjacent SOFC components, thus potentially causing CTE-mismatch-induced cracking/damage in the SOFC stacks.

The E-brite itself contained a small amount of Mn, and Mn was able to diffuse through the Cr_2O_3 scale into the Co_3O_4 spinel layer. However, the amount of Mn in the spinel was limited, due to the low level of Mn in the alloy substrate. On the contrary, due to additional Mn incorporation from the Mn_3O_4 particles, the converted Co-Mn_3O_4 coating had a much higher Mn content after 4 h conversion, compared to the converted Co coating, as is clearly shown in Figures 6(b) and 6(d).

Electro-codeposited composite coatings were used to enhance the oxidation/corrosion resistance of metal, including a Ni (or Ni-Co) matrix embedded with metallic particles such as Al and CrAlY, which requires a diffusion treatment in an inert environment to convert the composite layer into a multiphase coating via the interdiffusion between the metal matrix and the embedded metallic particles [19–21]. The current work involves the complex reaction between a metal matrix, embedded oxide particles, and oxygen in the conversion environment to form a single-phase spinel oxide coating. Furthermore, during the conversion process, interdiffusion between the coating and the metallic substrate will occur and an oxide scale can be formed at the coating-substrate interface. From what has been discussed above, the process of thermal conversion of the Co-Mn_3O_4 composite coating to the $(Co,Mn)_3O_4$ spinel layer can be described using the sketches in Figure 7, where the complex interactions among the substrate, the matrix, and the embedded phases in the composite coating and the environment are highlighted for eventual $(Co,Mn)_3O_4$ spinel coating formation.

4. Conclusion

The Co-Mn_3O_4 composite coating was successfully applied onto the FSS E-brite substrate by electro-codeposition, and the Mn_3O_4 particles were distributed uniformly in the coating. While after 10 min conversion at 800°C in air, a double-layer Co_3O_4/CoO structure with undissolved Mn_3O_4 particles was observed, and it was fully converted into the $(Co,Mn)_3O_4$ spinel coating after the 4 h treatment. Compared to the Co_3O_4 coating derived from the pure Co-plated layer, the thermally grown Cr_2O_3 scale at the coating/substrate interface was more compact and contained less Fe for the $(Co,Mn)_3O_4$ coating, which is beneficial for the application of the process for the enhancement of the corrosion resistance of the SOFC interconnects. The Co diffusion from the coating to the substrate may have a negative impact on the coating performance due to the potential CTE mismatch caused by the formation of the Co-containing FCC region near the coating/substrate interface.

Data Availability

The data used to support the findings of this study are available from the corresponding author upon request.

Conflicts of Interest

The authors declare that they have no conflicts of interest.

Acknowledgments

This work was supported by the National Natural Science Foundation of China under Grant no. 11204199 and Shanxi Scholarship Council of China under Grant no. 2016-096.

References

[1] X. Chen, P. Y. Hou, C. P. Jacobson et al., "Protective coating on stainless steel interconnect for SOFCs: oxidation kinetics and electrical properties," *Solid State Ionics*, vol. 176, no. 5-6, pp. 425–433, 2005.

[2] W. N. Liu, X. Sun, E. Stephens et al., "Life prediction of coated and uncoated metallic interconnect for solid oxide fuel cell applications," *Journal of Power Sources*, vol. 189, no. 2, pp. 1044–1050, 2009.

[3] M. Bobruk, S. Molin, M. Chen et al., "Sintering of $MnCo_2O_4$ coatings prepared by electrophoretic deposition," *Materials Letters*, vol. 213, pp. 394–398, 2018.

[4] S. J. Geng and J. H. Zhu, "Promising alloys for intermediate-temperature solid oxide fuel cell interconnect application," *Journal of Power Sources*, vol. 160, no. 2, pp. 1009–1016, 2006.

[5] J. H. Zhu, S. J. Geng, and D. A. Ballard, "Evaluation of several low thermal expansion Fe–Co–Ni alloys as interconnect for reduced-temperature solid oxide fuel cell," *International Journal of Hydrogen Energy*, vol. 32, no. 16, pp. 3682–3688, 2007.

[6] J. Pu, J. Li, B. Hua et al., "Oxidation kinetics and phase evolution of a Fe–16Cr alloy in simulated SOFC cathode atmosphere," *Journal of Power Sources*, vol. 158, no. 1, pp. 354–360, 2006.

[7] Z. Yang, G. G. Xia, X. H. Li et al., "$(Mn,Co)_3O_4$ spinel coatings on ferritic stainless steels for SOFC interconnect applications," *International Journal of Hydrogen Energy*, vol. 32, no. 16, pp. 3648–3654, 2007.

[8] H. Zhang, Z. L. Zhan, and X. B. Liu, "Electrophoretic deposition of $(Mn,Co)_3O_4$ spinel coating for solid oxide fuel cell interconnects," *Journal of Power Sources*, vol. 196, no. 19, pp. 8041–8047, 2011.

[9] S. P. Jiang and X. B. Chen, "Chromium deposition and poisoning of cathodes of solid oxide fuel cells—a review," *International Journal of Hydrogen Energy*, vol. 39, no. 1, pp. 505–531, 2014.

[10] A. Kruk, M. Stygar, and T. Brylewski, "Mn–Co spinel protective–conductive coating on AL453 ferritic stainless steel for IT-SOFC interconnect applications," *Journal of Solid State Electrochemistry*, vol. 17, no. 4, pp. 993–1003, 2013.

[11] Q. Fu, F. Tietz, D. Sebold et al., "Magnetron-sputtered cobalt-based protective coatings on ferritic steels for solid oxide fuel cell interconnect applications," *Corrosion Science*, vol. 54, pp. 68–76, 2012.

[12] T. Brylewski, J. Dabek, K. Przybylski et al., "Screen-printed $(La,Sr)CrO_3$ coatings on ferritic stainless steel interconnects for solid oxide fuel cells using nanopowders prepared by means of ultrasonic spray pyrolysis," *Journal of Power Sources*, vol. 208, pp. 86–95, 2012.

[13] M. R. Bateni, P. Wei, X. H. Deng et al., "Spinel coatings for UNS 430 stainless steel interconnects," *Surface and Coatings Technology*, vol. 201, no. 8, pp. 4677–4684, 2007.

[14] J. W. Wu, Y. L. Jiang, C. Johnson et al., "DC electrodeposition of Mn–Co alloys on stainless steels for SOFC interconnect application," *Journal of Power Sources*, vol. 177, no. 2, pp. 376–385, 2008.

[15] S. Apelt, Y. Zhang, J. H. Zhu et al., "Electrodeposition of Co-Mn_3O_4 composite coatings," *Surface and Coatings Technology*, vol. 280, pp. 208–215, 2015.

[16] M. Chen, B. Hallstedt, and L. J. Gauckler, "Thermodynamic assessment of the Co-O system," *Journal of Phase Equilibria*, vol. 24, no. 3, pp. 212–227, 2003.

[17] S. Velraj, J. H. Zhu, A. S. Painter et al., "Impedance spectroscopy of the oxide films formed during high temperature oxidation of a cobalt-plated ferritic alloy," *Journal of Power Sources*, vol. 247, pp. 314–321, 2014.

[18] Z. H. Bi, J. H. Zhu, S. W. Du et al., "Effect of alloy composition on the oxide scale formation and electrical conductivity behavior of Co-plated ferritic alloys," *Surface and Coatings Technology*, vol. 228, pp. 124–131, 2013.

[19] B. L. Bates, L. Z. Zhang, and Y. Zhang, "Electrodeposition of Ni matrix composite coatings with embedded CrAlY particles," *Surface Engineering*, vol. 3, no. 3, pp. 202–208, 2015.

[20] Y. Zhang, "Electrodeposited MCrAlY coatings for gas turbine engine applications," *JOM*, vol. 67, no. 11, pp. 2599–2607, 2015.

[21] L. Z. Zhang, B. L. Bates, and Y. Zhang, "Effect of post-deposition heat treatment on electrodeposited NiCoCrAlY coatings," *Surface Engineering*, vol. 33, no. 2, pp. 136–141, 2017.